Journal of Oral Biology and Craniofacial Research 14 (2024) 570–577

Contents lists available at ScienceDirect

Journal of Oral Biology and Craniofacial Research

journal homepage: www.elsevier.com/locate/jobcr

Computerised assessment-a novel approach for calculation of percentage of hypomineralized lesion on incisors and its correlation with aesthetic concern

Manojkumar Jaiswal [a,*], Umer Mukhtar [a], Kaushlesh Singh Shakya [b], Amit Laddi [c], L Akash Singha [a]

[a] A Unit of Pediatric and Preventive Dentistry, Oral Health Sciences Center, Postgraduate Institute of Medical Education and Research, Chandigarh, India
[b] Academy of Scientific & Innovative Research (AcSIR), Ghaziabad, India
[c] CSIR-Central Scientific Instruments Organisation, Chandigarh, India

ARTICLE INFO

Keywords:
MIH lesion
Artificial intelligence
Opacity calculation
Aesthetics

ABSTRACT

Introduction: Molar-incisor hypomineralization (MIH) is a localized, qualitative, demarcated enamel defect that affects first permanent molars (FPMs) and/or permanent incisors. The aim of present study was to introduce a novel computerised assessment process to detect and quantify the percentage opacity associated with MIH affected maxillary central incisors.

Methodology: Children (8–16 years) enrolled in the primary study having mild (white/cream or yellow/brown) MIH lesion on fully erupted maxillary permanent central incisor. 50 standardised images of MIH lesions were captured in an artificially lit room with fixed parameters and were anonymized and securely stored. Images were analysed by AI-driven computerised software and generates output classifications via a sophisticated algorithm crafted using a meticulously annotated image dataset as reference through supervised machine learning (SML). For the validation of computerised assessment of MIH lesions, the percentage of demarked opacity was calculated using *ADOBE PHOTOSHOP CS7*.

Results: The percentage of MIH lesion was calculated through histogram plotting with the maxima ranging from 7.29 % to 71.21 % with the mean value of 34.51 %. The validation score ranged from 10.29 % to 67.27 % with the mean value of 35.32 %. The difference between the two was statistically not significant. Out of 50 patients; 11 patients had 1–30 % of surface affected with MIH and 2 had aesthetic concern; 24 had 30–60 % of surface affected and 13 had aesthetic concern; 15 had >60 % of surface affected and 12 had aesthetic concerns.

Conclusions: The proposed approach exhibit sufficient quality to be integrated into a dental software addressing practical challenges encountered in daily clinical settings.

1. Introduction

Molar-incisor hypomineralization (MIH) is an enamel defect which presents clinically as a clearly demarcated opacities with an alteration in the translucency, showing a wide variation in colour, size, and shape that affects first permanent molars (FPMs) and/or permanent incisors leading to a significant reduction in mineral density of up to 20 %.[1] An imbalance in calcium and phosphorous ratio as well as reduced levels of proteases (KLK4 and MMP-20) and anti-proteases (anti-thrombin-III which inhibits KLK4) may be responsible for reduced mineralized effect on hypo-mineralized enamel (HE). Alterations in elemental and proteomic composition, increased porosity, and reduced mineral density of HE can affect its mechanical strength. This ultimately results in fragmentation and breakdown under the forces of mastication, which is called post-eruptive breakdown (PEB).[2]

While the opacities on anterior teeth may primarily cause cosmetic and psychosocial issues, treating incisors affected by MIH poses challenges due to variation in the presentation in terms of colour, extent and location of the opacities.[3] Existing treatment approaches ranges from minimally invasive to radical methods. However, objective methods to

* Corresponding author.
E-mail addresses: drmanojjaiswal@yahoo.in (M. Jaiswal), umermukhtar19@gmail.com (U. Mukhtar), kaushlesh.csio19a@acsir.res.in (K.S. Shakya), amitladdi@csio.res.in (A. Laddi), Akisingha007@Gmail.Com (L.A. Singha).

https://doi.org/10.1016/j.jobcr.2024.07.004
Received 15 April 2024; Received in revised form 9 July 2024; Accepted 16 July 2024

record the extent of these defects are lacking, hindering treatment planning and evaluation. Minimally invasive approaches such as micro-abrasion and resin infiltration face challenges due to the intact enamel layer acting as a barrier to accessing the lesion ceiling as described by Jeanne Pierre Attal et al., 2014.[4] Another obstacle is the method of evaluation of the effect of the intervention. Subjective methods such as photographic evaluation and clinical examination which are prone to bias and objective methods like a hand-held spectrophotometer to measure the L*, a*, b* values or employing CIELAB method to evaluate clinical photographs as well as software-based measurement of the areas of opacity in the clinical photographs and its change after the intervention have been explored but hasn't been established as the optimal approach.[5]

Computerised analysis via Artificial Intelligence (AI) is rapidly expanding across all sectors playing a comprehensive role in people's life. AI is now widely used in the field of medicine and dentistry for imaging diagnostics, decision support, precision and digital medicine, drug discovery, wearable technology, hospital monitoring, robotic and virtual assistants.[6]

Given the prevalence of oral health problems in children, early diagnosis, prevention, and treatment of these disorders are crucial for their optimal health. The ability of AI to enhance patient care and provide precise diagnoses have revolutionized the healthcare industry. In the field of pediatric dentistry, the capability to effectively execute treatment measures while also providing behaviour counselling is particularly sought after. MIH is one such dental condition which is under extensive research for risk factors, aetiology, diagnosis, and management. Various criteria's have been introduced in literature like Oliver criteria (2013), Ghanim criteria (2015) and EAPD (2003), but none of the existing criteria have objectively assessed the lesion extension. Computerised assessment of MIH lesions is one of the methods that could improve the efficacy of assessment of effectiveness of various minimally invasive treatment modalities such as micro-abrasion, resin infiltration, deproteinization and remineralization and may provide systematic evaluation of changes in such type of lesions.

Therefore, the objective of the present study is to introduce a novel computerised assessment process to detect and quantify the percentage opacity associated with MIH affected maxillary central incisors. By leveraging AI technology, this approach seeks to provide a more accurate and standardized method for evaluating MIH- related opacities thereby improving diagnosis and treatment outcome.

2. Materials and methods

2.1. Study design overview

This laboratory-based investigation was carried out in conjunction with a large-scale clinical study, which sought to explore the change in children with MIH following the aesthetic management of their incisor opacities. In the primary study, two investigators (NH and JL) treated children aged 8–16 years, who attended the Out-Patient Department of Paediatric and Preventive dentistry, Chandigarh, India followed by management of the incisor opacities. Children were clinically diagnosed with MIH according to Ghanim's criteria 2015.[7]

Standard intra-oral anterior clinical images were taken for each child pre-treatment by using a digital SLR camera (Nikon D3400; Nikon UK Ltd.) equipped with a Sigma EM 140DG macro ring flash (Sigma Imaging [UK] Ltd.) and Tamron 90-mm macro lens (TAMRON Europe GmbH). To ensure image capture standardisation, a modified method described by Murphy and colleagues was adopted.[8]

Ethical and collaborative clearance was obtained from Institute Ethics committee and institute collaborative research committee respectively (PGI/IEC/2022/E702). Standardised clinical photographs were captured in an artificially lit room with fixed parameters (Focal length 160, shutter speed 160, ISO sensitivity 160, White Balance, WB-Auto). The child's position was also standardized by making them sit upright, at a distance of 30 cms measured from the camera's focal plane mark, with positioning of the cheek retractors and the camera always positioned parallel to the child's frontal plane (Figure. a). A cut-out of grey card was put on the adjacent tooth for post-processing of the photos for removal of any colour cast (Figure. b).

The clinical digital images captured the appearance of the patients' affected teeth and were anonymized and securely stored. These images were used as the primary data for a lab study to create and validate a computerised process for assessing MIH lesions using AI-driven image analysis techniques. This lab study supports clinical research by offering an objective and standardized method to evaluate the severity and extent of MIH lesions, thereby enhancing the overall research framework.

2.2. Participants

Inclusion criteria: Children of age 8–16 years were enrolled in the primary study with at least one discrete, mild (white/cream or yellow/brown) MIH lesion present on at least one fully erupted maxillary permanent central incisor.

Exclusion criteria.

1. Children were excluded from the study if they had incisors with MIH that showed post-eruptive breakdown, partially erupted teeth, or any other developmental enamel defects.
2. Additionally, children with associated medical conditions or special healthcare needs were excluded to prevent potential confounding factors that could influence MIH assessment or treatment outcomes. These include systemic diseases, developmental disorders, or any medical issues that could affect oral health or the ability to follow study procedures.

2.3. Image analysis via artificial intelligence

Convenient sample of 50 MIH affected maxillary images were taken for computerised assessment. Sample size was calculated based on the pilot study done. AI-driven image analysis takes image data as input and generates output classifications based on predefined rules, ranging from straightforward expert-derived logic to more intricate algorithms.[8] In contrast, supervised machine learning (SML) employs a distinct methodology where raw data, such as digital images, undergo interpretation via a sophisticated algorithm crafted using a meticulously annotated image dataset as reference. SML encompasses a diverse array of algorithms, with convolutional neural networks (CNNs) standing out as a popular choice for their effectiveness in image analysis. [8]The process of analyzing photographic images proceeded as follows:

2.3.1. Procedures for image standardization

Image standardization refers to the process of comparing a digitized image to a reference or an image that is considered to be of an optimal quality.[9,10] There are several algorithms that are available for comparing images, which are designed to ensure the reproduction of high-quality images.[11–13] Images of the oral cavity are commonly affected by inconsistent lighting, which can result in variations in brightness and darkness depending on the capturing conditions. To rectify these issues, it is essential to -

- Correct shading inconsistencies
- Standardize grey values
- Ensure an appropriate range of grey values (typically 8 bits).[13,14]

These corrective measures can be categorised as locally dependent filters and can be applied to both the original images and their derivatives. The derivative image is mainly used in segmentation algorithms. Differences in filter parameters serve as indicators of image quality, with smaller parameters indicating better quality.[13] These

Figure a. Represents Standardised clinical photographs capturing in an artificially lit room in a fixed position using a digital camera, ring flash, macro lens, contrast, tripod stand.

Figure b. GREY CARD -with a set chromatic parameter was used for standardisation.

algorithms were implemented separately for each color space, especially in cases involving images in the red-green-blue (RGB) color space. Once the image has been corrected and standardized, it is ready for further analysis.

2.3.2. Assessment of potential segmentation threshold

Various techniques are utilized for dividing an image into multiple segments, including edge, color, gradient, region-based, and dynamic segmentation.[15,16,17] All of these techniques rely on differences in grey values with varying effectiveness. The differences in grey-value intensities are correlated with the segmentation accuracy and can be represented through grey-value histograms.[10]Additional, techniques include -

- Converting the image to LAB color space (L* indicates lightness, a* is the red/green coordinate, and b* is the yellow/blue coordinate)
- Calculating the mean luminance of a marked area
- Adjusting the luminance values to match the mean luminance.[18]

The CIELAB color space (also known as LAB) is a color-opponent space with three coordinates: L* for lightness, and a* and b* for the color-opponent dimensions. It was designed to be perceptually uniform, meaning that the same amount of numerical change in these values corresponds to about the same amount of visually perceived change.

The potential segmentation thresholds in both unaltered and processed standardized images from a standard calibration tile was done as illustrated in Figure.c.

2.3.3. Texture analysis

Texture analysis and structure assessment are two distinct concepts. Structure refers to how objects are arranged in space and relies on external understanding. Texture, conversely, pertains to the distribution of grey values at the pixel level and is independent of external factors.[12,19] The texture is more challenging to define precisely and often requires intricate formulas or locally dependent and independent image transformations.[20,21] Established techniques like Fourier, Hough, and Hadamard transformations, k-means clustering, and gradient-based operations such as thinning, erosion, and dilation are commonly used.[21] Texture analysis allows for the evaluation of image-related features without prior knowledge. However, it is heavily dependent on image size, and its results are typically helpful for image comparison, particularly across different diagnoses. K-means clustering is a method that identifies patterns based on similarity, often using distance metrics like Euclidean distance. This iterative approach assigns data points to the nearest cluster centroid and updates the centroids until convergence. It plays a pivotal role in the development of automated pattern analysis algorithms.[22]

2.3.4. Segmentation algorithms

After standardizing the image and confirming suitable grey values for segmentation, it becomes necessary to identify objects within the region of interest (ROI). Histological images have two distinct areas: regions that may contain objects (also known as object spaces) and regions without objects commonly referred to as the background.[23] Usually, a simple grey-value thresholding method is sufficient to separate the pattern space, which is then further analysed for opacity differentiation and identification. The authors used a technique similar to non-random dynamic sampling, which involves applying variable grey value thresholds to draw object boundaries, along with features from neighboring objects that are clearly identified.

2.3.5. Finding Maxima for MIH

MIH lesion analysis process was carried out in a sequence of steps as shown in (Figure.d).

Original Image→ Calibration Tile→ Calibrated Image→ Selected MIH ROI→ROI Threshold→ ROI Histogram→Finding Maxima for MIH.

Image Processing: The code used the OpenCV library to read and manipulate images. It converts the image to the LAB color space, determines the mean luminance of a selected area, and adjusts the luminance values to match this mean.

ROI Selection: The code allows the user to select a Region of Interest

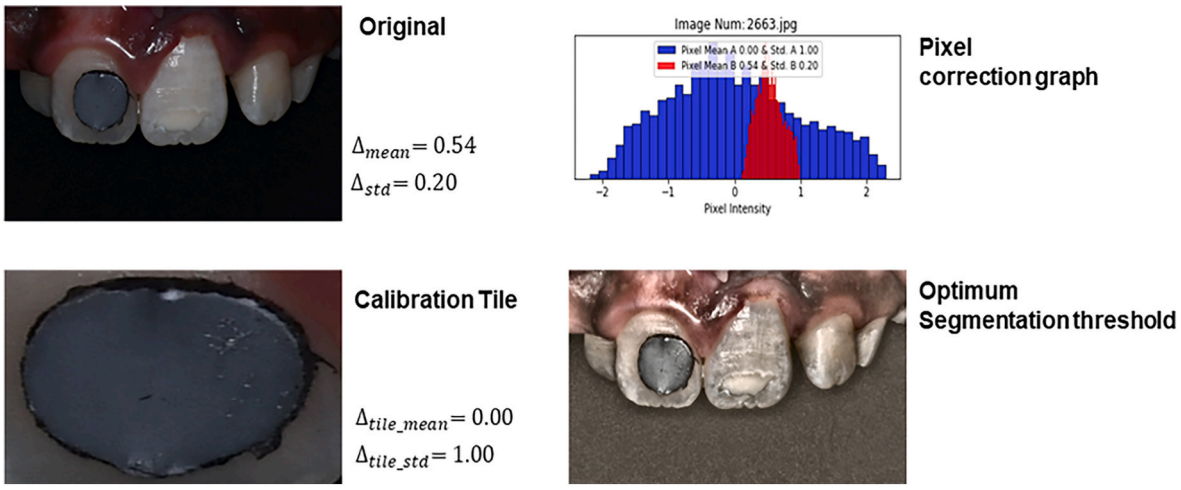

Figure c. Impact of Shading Correction on Segmentation Processes: This figure illustrates the potential segmentation thresholds in both unaltered and processed standardized images from a standard calibration tile. The original image of the dental sample is shown alongside a pixel-correction graph, which quantitatively illustrates the correction applied to the pixel intensities. This graph shows the distribution of pixel values before and after correction, providing a precise quantitative analysis of the shading correction process. The calibration tile image is included to show the reference standard used for correction, and the accompanying Δ_tile values (mean and standard deviation) provide a baseline for evaluating the effectiveness of the correction algorithm. In addition, the post-segmentation image illustrates the final result of the algorithm, and when combined with the quantitative metrics provided (Δ_mean and Δ_std), it offers a detailed evaluation of the segmentation quality. The number and height of the evaluated grey value thresholds serve as additional indicators of image quality.

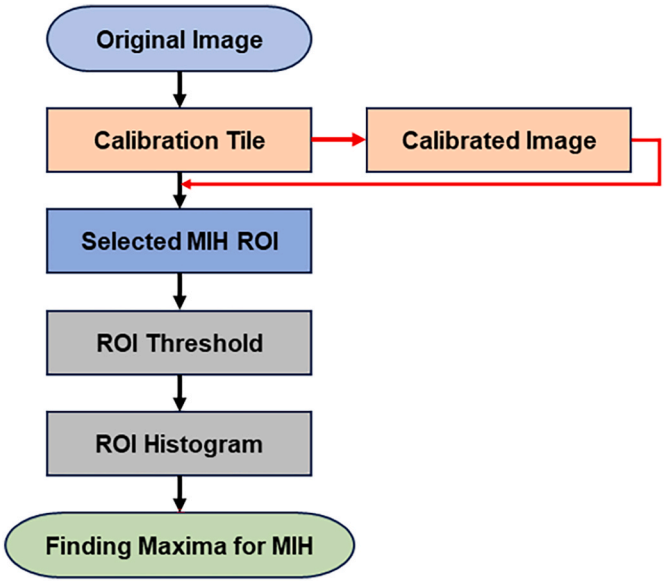

Figure d. Flow chart of various steps of MIH lesion analysis process.

(ROI) by clicking and dragging the mouse. The desired ROI is then used for further analysis. The code extracts pixel values (color information) from the ROI and stores them in a CSV file.

Clustering: The K-means clustering algorithm groups the pixel values into different clusters based on similarity. The clustered data is then visualized by creating separate images for each cluster. After the initial analysis, the code prompts the user to choose a specific image or option, which determines the further processing and visualization of the data. A simple graphical user interface (GUI) is implemented using the Tkinter library to provide the user with options.

Anomaly Calculation: Based on the clustering results, the code calculates the anomaly percentage by comparing the sizes of the two clusters. The anomaly percentage indicates the extent of abnormality or dissimilarity in the selected ROI (Figure.e).

2.3.6. Validation

For the validation of computerised assessment of MIH lesions, the percentage of demarked opacity was calculated using *ADOBE PHOTOSHOP CS7*. Adobe Photoshop CS7 was used because of its strong image processing capabilities and wide availability, making it a practical choice for both clinical and research settings. Adobe Photoshop CS7 provides advanced tools for precise image manipulation and analysis, ensuring accuracy in measuring marked opacity providing a reliable benchmark for evaluating MIH lesions.

The validation process involved calculating the percentage of marked opacity using Adobe Photoshop CS7. Grids were applied to the digital images to aid in manual counting, allowing for a detailed comparison of the computerised analysis results with manual assessments. This step is crucial for establishing the reliability of the automated system (Figure.f).

2.3.6.1. Maxima determination. To determine if a pixel (x,y) is a local maximum within a neighborhood window, we compare its intensity value $I(x,y)$ with the intensity values of all neighboring pixels (a,b) within the window using the equation:

$I(x,y) > I(a,b)$ for all (a,b) in the neighborhood window.

2.3.6.2. Ratio calculation. To assess the distribution of pixel values in an image, we use equations to evaluate the prevalence of high and low pixel values and their correlation with defects.

1. Calculate the number of high pixels:

The number of pixels exhibiting high intensity values is determined by the equation:

$$DefectHigh[i-215] = \sum_{i=215}^{255} (I(x,y) == i) \quad (1)$$

where i iterates over intensity values from 215 to 255, and $I(x,y)$ represents the pixel value at coordinates (x,y) in the image. This summation yields the total count of high pixels.

2. Calculate the number of low pixels:

Similarly, the count of pixels with low intensity values is computed

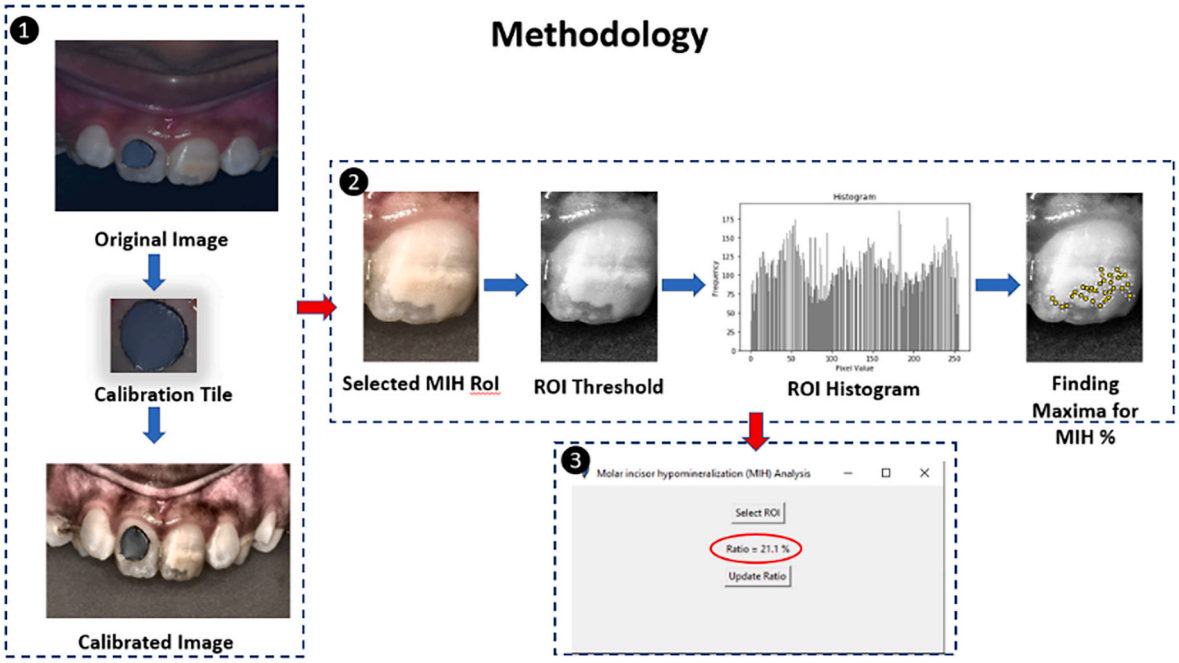

Figure e. Represents graphical user interface (GUI) implemented using Tkinter library. Based on the clustering results, the code calculates the anomaly percentage by comparing the sizes of the two clusters. The anomaly percentage indicates the extent of abnormality or dissimilarity in the selected ROI.

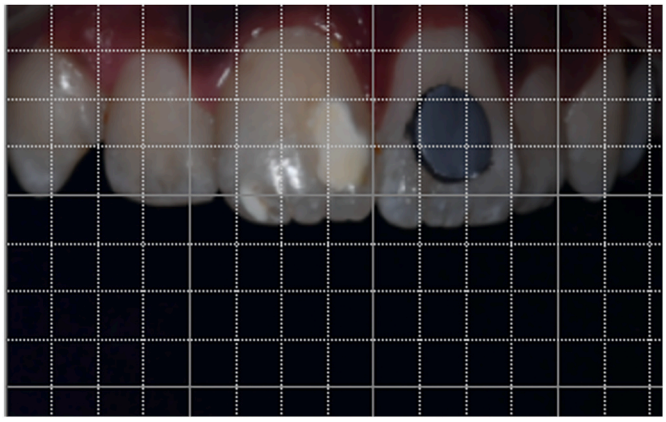

Figure f. Calculation of percentage of demarked opacity using *ADOBE PHOTOSHOP CS7* software, by applying grids on the digital images.

using:

$$Defectlow[j-60] = \sum_{j=60}^{214} (I(x,y) = = j) \quad (2)$$

where j ranges from 60 to 214. The summation across this range provides the total count of low pixels.

3. Calculate the total number of high and low pixels:

The total number of defective pixels, encompassing both high and low intensity values, is obtained by summing the counts from the previous steps:

$$TotalDefect = \sum Defectlow[j-60] + \sum Defecthigh\,[i-215] \quad (3)$$

This cumulative count represents the overall extent of defects within the image.

4. Calculate the ratio of high pixels to total defects:

Finally, to assess the relative prevalence of high-intensity pixels among all defects, we compute the ratio:

$$Ratio = \left(\frac{totaldefecthigh}{totaldefect}\right) \times 10 \quad (4)$$

total defect high Denotes the count of high-intensity pixels, and *totaldefect* represents the total count of defective pixels. Scaling the ratio by a factor of 10 facilitates comparison and interpretation of the severity of defects attributed to high pixel values.

2.4. Intra-operator repeatability

All image analysis was undertaken by one investigator, and intra-operator repeatability was determined by repeating the quantification process with 1- to 8-week interval on 20 % (n = 10) of the images. Intra-class correlation coefficients (ICC) was calculated to determine the level of agreement between the first and repeat MIH lesion calibration and validation on labial surface of maxillary central and was found to be 0.84.

2.5. Statistical analysis

Data was entered in MS Excel spreadsheets and imported to IBM SPSS v25.0, Armonk, NY: IBM Corp for further analysis. Variables on the continuous scale were tested for normality using Shapiro Wilk test. Bivariate analysis involving means were compared using unpaired *t*-test after testing for normal distribution. Bivariate analysis of categorical variables was done using Chi-square test.

Level of significance was decided at a p-value <0.05 for all statistical inferences.

3. Results

3.1. Demographic characteristics

In the present study, 50 standardised images of MIH affected maxillary central incisors were analysed. Their age ranged from 8 to 16 years with the mean age of 10.97 years. Among the 50 patients; 62 %(n

= 31) were male and 38 %(19) were females.82 % of the cases displayed white/creamy coloured lesions, while the remaining 18 % cases exhibited yellowish/brown coloration in the MIH lesion (Table .1).

3.2. MIH lesion analysis findings

The percentage of MIH lesion was calculated through histogram plotting with the maxima ranging from 7.29 % to 71.21 % with the mean value of 34.51 %. The validation score ranged from 10.29 % to 67.27 % with the mean value of 35.32 %. The difference between the two was statistically not significant (p = 0.7186) (Figure. g).

The Specular artefact, resulting due to artificial light was measured and categorised into three sub-sets; type I) 0–5%, type II) 5–15 %, type III)15–30 %. Among 50 images, 31 fell in type I (0–5%) with an accuracy range of 91%–97 % (average accuracy = 94 %) and precision value of 89 %. 11 images showed specular artefact of type II (5–15 %) with accuracy range of 79%–83 % (average accuracy = 81 %) and precision value of 64 %. Remaining 8 images showed specular artefact of type III (15%–30 %) with accuracy range of 56%–59 % (average accuracy = 57 %) and precision value of 45 % (Table 2).

Based on the percentage of MIH lesion extension on the tooth surface, the patients were divided into 3 categories. Aesthetic concern was found to correlate with the extension of the lesion (Table 3). Out of 50 patients; 11(22 %) were found to have 1–30 % of surface affected with MIH and only 2 of them had aesthetic concern; 24(48 %) had 30–60 % of surface affected and among them 13(54 %) had aesthetic concern; 15 (30 %) had >60 % of surface affected with MIH with 12(80 %) patients having aesthetic concerns (Table 3). All patients underwent various treatment modalities including micro-abrasion with etching, micro-abrasion with deproteinization with 5.5 % NaOCl, followed by remineralization with GC Tooth Mousse, resin-infiltration, composite restoration depending upon the patient need. Some dental images contained specular reflections from light on the tooth surface that gives artefact and were picked up for the lesion extension.

The variation in the percentage of brown lesion in image 2 and image 8 might be due to partial identification of extension of MIH lesion. Among 9 brown lesions two images showed large difference in the extension of lesion between histogram and validation method due to unknown reasons (Figure.h).

4. Discussion

Using computerised image analysis, the present study aimed to objectively assess the extension of MIH lesions on the labial surfaces of maxillary incisors and its correlation with the aesthetic concern of the patient. Recording the extent of the defect associated with MIH affected incisors subjectively or objectively can serve the purpose of categorising the defects in terms of severity according to their extent. Reports in the literature have suggested that the extent of the MIH lesion tends to increase with the severity of the lesion thus categorising the lesion severity according to its extent seems to be logical. Ghanim's criteria 2015 categorises all lesions irrespective of their colour and extent in the mild category unless associated with complications like post-eruptive breakdown, atypical restorations and atypical caries.[7]Another common criteria Oliver's criteria 2013, categorises the MIH lesions as mild, moderate and severe is the but lacks the provision of categorising the

Table 1
Distribution of MIH affected incisors based on age, gender and colour of MIH lesion of included patients.

Opacity Colour		Mean age of patients (8–16 years) (mean ± SD)	Gender(n = 50)	
			Males	Females
White/ creamy 41(82 %)	**Yellow/ brown** 9 (18 %)	10.97 ± 2.04years	31(62 %)	19(38 %)

Table 2
Percentage of specular artefact and accuracy of histogram while analysis of MIH lesions on selected images.

Categories of Specular artefact	Percentage of Specular Artefact	No. of Images (N = 50)	Accuracy	Average Accuracy	Precision
Type I	0–5 %	31(62 %)	91 %–97 %	94 %	89 %
Type II	5–15 %	11(22 %)	79 %–83 %	81 %	64 %
Type III	15–30 %	8(16)	56 %–59 %	57 %	45 %

This table represents specular artefact that was calculated by computer with accuracy and precision values and based on the percentage of artefact; images were categorised into the three sub-sets; type I) 0–5%, type II) 5–15 %, type III) 15–30 %.

based on extent.[24] The present study objectively assesses the extension of MIH lesions on the labial surfaces of maxillary incisors and its correlation with the aesthetic concern of the patientand categorising based on extent. The greyscale pixel intensity of normal and hypomineralised (area of opacity) enamel was used to objectively determine opacity visibility.

Similarly, Kanthathas K et al. (2005)employed computerised image analysis for exploring interventions to improve the aesthetics of post-orthodontic demineralised lesions and developmental enamel defects.[25] In the present study, 82 % of the images showed an accuracy of 81 % in lesion extent of lesion deemed acceptable for calibration. Specular artefact up to 15 % was deemed acceptable, beyond which the accuracy gets significantly reduced.Based on the percentage of extent of MIH lesion, it was found that if the lesion extended above 20 % of the anterior tooth surfaces, 60 % of parents and 63 % of children expressed aestheticconcern. This correlation between lesion extent and aesthetics has not been evaluated in existing literature to the best of our knowledge. AI offers advantages such as homogenous and uniform categorization of % extension of MIH lesion on the anterior teeth, aiding in aesthetic intervention.

Assessing the effects of intervention on MIH affected incisors involves both qualitative evaluation of colour change and quantitative evaluation ofopacity size reduction. Qualitative methods like CIELAB method and spectrophotometer measure the colour change while quantitative methods calculate the size reduction of opacities as employed by Warner et al.(2021).[5]

The method described in present study offers a quantitative approach for evaluation of impact of interventions on incipient carious lesions and mild developmental defects after remineralization. However, a limitation in evaluating developmental defects via computerised image analysis, is unwanted reflections despite the use of accessories like ring flash. These reflections can result in overestimation of the size of the defects or inconsistencies in the recording of color parameters.

Hasmun and colleagues (2020) used a theoretical model and validated measure of OHRQoL to assess child reported outcomes post-minimally invasive aesthetic management, showing a significant improvement 6 months after treatment.[26] Alongside patient-reported outcome measures, such as OHRQoL, it is also crucial to develop clinical outcome measures for objectively measuring treatment 'success', and informing the assessment of new materials and techniques.[10] Variation in the clinical presentation of hypomineralised permanent anterior teeth may account for the broad spectrum of treatment regimens offered to children, which essentially aims to mask, remove, or cover the affected enamel.[26]Addressing the impact of these reflections, this study calculated the specular reflection percentage, finding that accuracy significantly decreases when the specular artefact is above 15 %. Clinical relevance lies in thoroughly considering two parameters: a reduction in opacity size and a reduction in the maximum pixel intensity (whiteness/brightness) of the treated area.

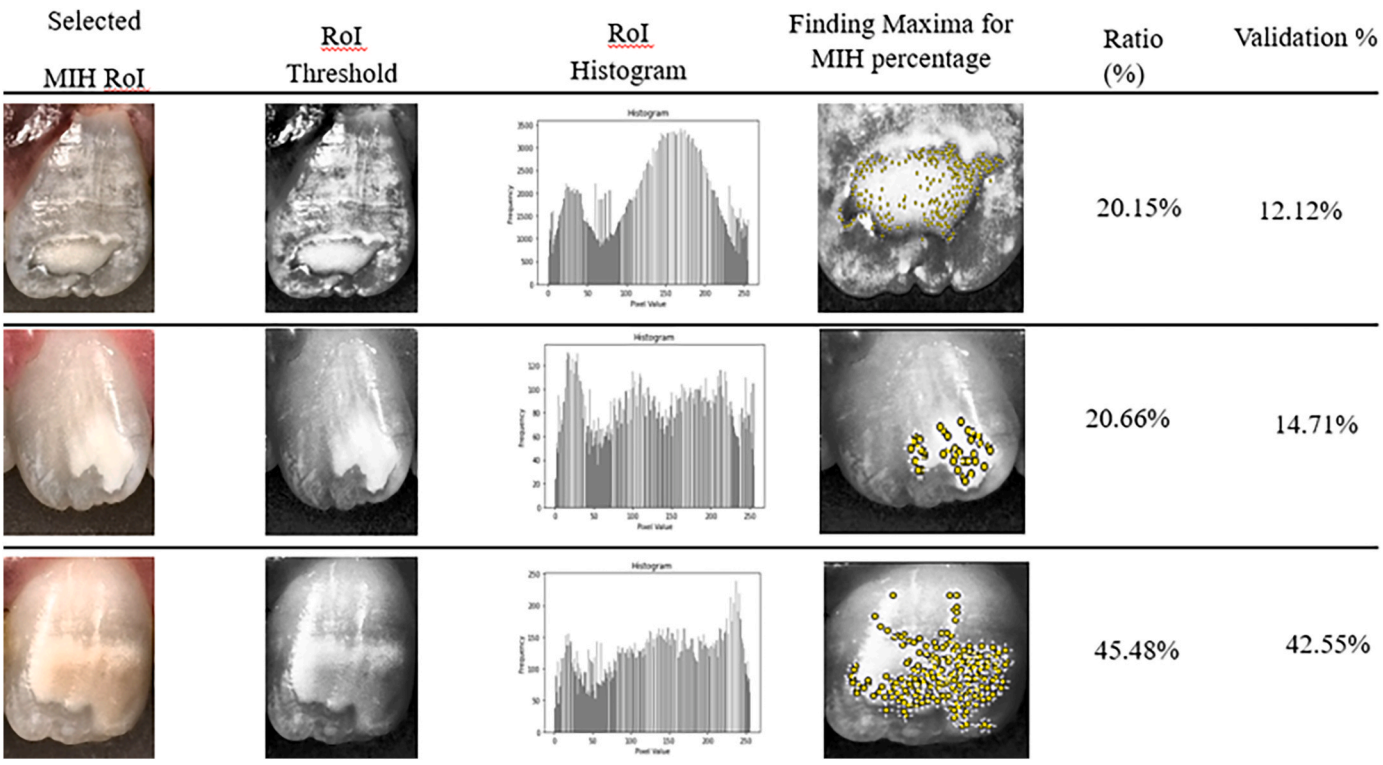

Figure g. Represents histogram of region of interest of MIH lesion selected from standardized image and measurement of maxima and ratio and validation value percentage.

Table 3
Distribution of patients based on the percentage of MIH lesion and aesthetic concern and correlation between lesion extension and aesthetic concern of patient/parent.

% of MIH lesion extension	No. Patients (n = 50)	Patients with aesthetic concern	*p*-value
Category I (1–30 %)	11(22 %)	2/11(18.18 %)	0.196
Category II (30–60 %)	24(48 %)	13/24(54.16 %)	
Category III (>60 %)	15(30 %)	12/15(80 %)	
Total	50	27/50(54 %)	

(Chi-square = 3.2).

This study identified several significant limitations. Specular reflections posed difficulties in accurately delineating the affected dental region, possibly leading to inaccurate MIH ratio calculation. Additionally, these artefacts also affected the histogram analysis and MIH calculation, potentially misleading the outcomes. Furthermore, AI algorithms employed may have exhibited bias influenced by factors such as diverse enamel opacity patterns, lighting conditions during image capture, and demographic variations that affect aesthetic perceptions. These limitations warrant improvement in future research.

5. Conclusion

Based on the observations of this study, the proposed software can

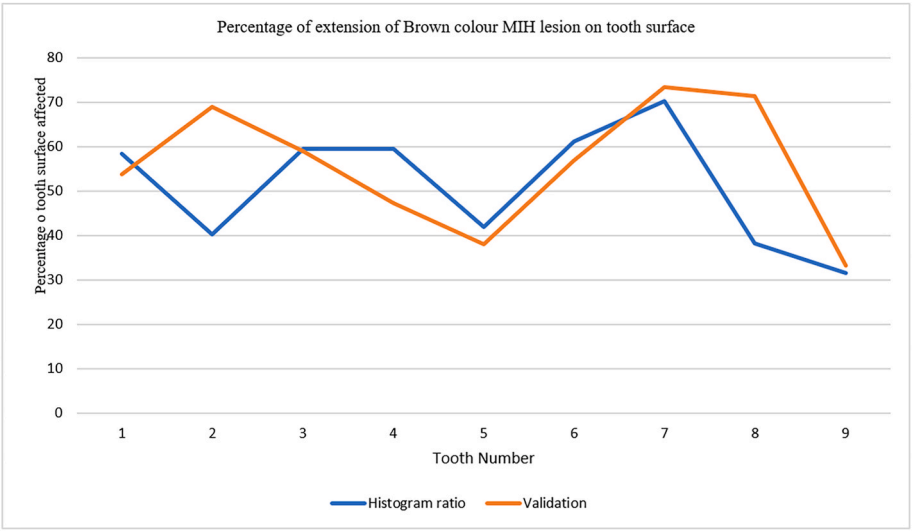

Figure h. Histogram represents comparative assessment of percentage extension of Brown coloured MIH lesion on Labial surface of maxillary central incisors.

assist clinicians plan the treatment of MIH-affected incisors for remineralization/active treatment with resin infiltration, Micro abrasion, Bleaching, veneers, composite restorations. The experimental results demonstrate that the proposed approach exhibits sufficient quality to be integrated into a dental software solution, addressing practical challenges encountered in daily clinical settings. Further research is warranted to address the identified limitations and improve the accuracy of the proposed approach, which can also be extended to encompass multiple classifications in the future.

Consent

Patients parents/guardians were informed that they were enrolled in a study and consent was taken from all Patient's parents/Guardians and only those patients who give consent were included.

Ethical clearance

Ethical and collaborative clearance was obtained from institute ethical committee and institute collaborative research committee respectively (PGI/IEC/2022/E702).

Source of funding

No source of Funding

Declaration of competing interest

There are no conflicts of interest.

Acknowledgements

Nil.

References

1. Fearne J, Anderson P, Davis GR. 3D Xray microscopic study of the extent of variations in enamel density in first permanent molars with idiopathic enamel hypomineralisation. *Br Dent J*. 2004;196:634–638.
2. Mukhtar U, Goyal A, Luthra-Guptasarma M, Gauba K, Kapur A, Thakur AK. Label-free quantitative proteomics reveals molecular correlates of altered biomechanical properties in molar incisor hypomineralization (MIH): an in vitro study. *Eur Arch Paediatr Dent*. 2022;23(1):179–191. https://doi.org/10.1007/s40368-021-00687-2.
3. Rodd HD, Graham A, Tajmehr N, Timms L, Hasmun N. Molar incisor hypomineralisation: current knowledge and practice. *Int Dent J*. 2021;71(4): 285–291. https://doi.org/10.1111/idj.12624.
4. Jean-Pierre Attal, Atlan Anthony, Denis Maud, Vennat Elsa, Tirlet Gilles. White spots on enamel: treatment protocol by superficial or deep infiltration (part 2). *Int Orthod*. 2014;12(1):1–31. https://doi.org/10.1016/j.ortho.2013.12.011.
5. Warner C, Hasmun NN, Elcock C, Lawson JA, Vettore MV, Rodd HD. Making white spots disappear! Do minimally invasive treatments improve incisor opacities in children with molar-incisor hypomineralisation? *Int J Paediatr Dent*. 2022;32(4): 617–625. https://doi.org/10.1111/ipd.12940.
6. Ding Hao, Wu Jiamin, Zhao Wuyuan, Matinlinna Jukka P, Burrow Michael F, James KH. Tsoi Artificial intelligence in dentistry—a review Front. Dent. Med, sec. *Dent Mater*. 2023;4. https://doi.org/10.3389/fdmed.2023.1085251.
7. Ghanim A, Elfrink M, Weerheijm K, Mariño R, Manton D. A practical method for use in epidemiological studies on enamel hypomineralisation. *Eur Arch Paediatr Dent*. 2015;16(3):235–246. https://doi.org/10.1007/s40368-015-0178-8.
8. Smith KP, Wang H, Durant TJ, et al. Applications of artificial intelligence in clinical microbiology diagnostic testing. *Clin Microbiol Newsl*. 2020;42:61–70.
9. He Lei, Rodney Long L, Antani Sameer, Thomas George R. Histology image analysis for carcinoma detection and grading. *Comput Methods Progr Biomed*. 2012;107(3): 538–556.
10. Kayser K, Gäśrtler J, Bogovac M, et al. AI (artificial intelligence) in histopathology–from image analysis to automated diagnosis. *Folia Histochem Cytobiol*. 2009;47(3): 355–361.
11. Gortler J, Berghoff M, Kayser G, et al. Grid technology in tissue- based diagnosis: fundamentals and potential developments. *Diagn Pathol*. 2006;1:23.
12. Saravanan Chandra, Schumacher Vanessa, Brown Danielle, et al. Meeting report: tissue-based image analysis. *Toxicol Pathol*. 2017;45(7):983–1003.
13. Jara-Lazaro, Richelia Ana, Thamboo Thomas Paulraj, Teh Ming, Tan Puay Hoon. Digital pathology: exploring its applications in diagnostic surgical pathology practice. *Pathology*. 2010;42(6):512–518.
14. Kayser K, Kayser G. Virtual microscopy and automated diagnosis. In: Gu J, Ogilvie R, eds. *Virtual Microscopy and Virtual Slides in Teaching, Diagnosis and Research*. Edition vol. 1. Boca Raton: Taylor & Francis; 2005:376. https://doi.org/10.1201/9781420039306.
15. Falah R, Bolon P, Cocquerez J. A region–region and region-edge cooperative approach of image segmentation. *International Conference on Image Processing*. October, 1994;3:470–474.
16. Lemoigne J. J Tilton Refining image segmentation by integration of edge and region data. *IEEE Trans Geosci Rem Sens*. 1995;33(3):605–615.
17. Chan F, Lam F, Poon P, Zhu H, Chan K. Object boundary location by region and contour deformation IEEE Proceedings—Vision Image and. *Signal Process*. 1996;143 (6):353–360.
18. Zollmann S, Kalkofen D, Mendez E, Reitmayr G. Image-based ghostings for single layer occlusions in augmented reality. In: *2010 IEEE International Symposium on Mixed and Augmented Reality*. 2010:19–26.
19. Elazab Naira, Soliman Hassan, El-Sappagh Shaker, Islam SM Riazul, Elmogy Mohammed. Objective diagnosis for histopathological images based on machine learning techniques: classical approaches and new trends. 2020;11:1863.
20. Kayser K, Molnar B, Weinstein R. *Virtual Microscopy: Fundamentals, Applications, Perspectives of Electronic Tissue Based Diagnosis*. Berlin: VSV Interdisciplinary Medical Publishing; 2006.
21. Kayser Klaus. Quantification of virtual slides: approaches to analysis of content-based image information. *J Pathol Inf*. 2011;2;1(2).
22. Linder Nina, Konsti Juho, Turkki Riku, et al. Identification of tumor epithelium and stroma in tissue microarrays using texture analysis. *Diagn Pathol*. 2012;7:1–11.
23. Kayser Klaus, Kayser Gian. Quantitation of immunohistochemistry by image analysis technique. *Technical Aspects of Toxicological Immunohistochemistry: System Specific Biomarkers*. 2016:51–71.
24. Oliver K, Messer LB, Manton DJ, et al. Distribution and severity of molar hypomineralisation: trial of a new severity index. *Int J Paediatr Dent*. 2014;24(2): 131–151. https://doi.org/10.1111/ipd.12040.
25. Kanthathas K, Willmot DR, Benson PE. Differentiation of developmental and post-orthodontic white lesions using image analysis. *Eur J Orthod*. 2005;27(2):167–172.
26. Hasmun N, Vettore MV, Lawson JA, Elcock C, Zaitoun H, Rodd HD. Determinants of children's oral health-related quality of life following aesthetic treatment of enamel opacities. *J Dent*. 2020;98, 103372. https://doi.org/10.1016/j.jdent.2020.103372.